

Experimental and analytical studies of base pipe pin connections under direct tension

Ali Mehrsoroush*, M. Saiid Saiidi

Department of Civil and Environmental Engineering, University of Nevada Reno, Reno, NV 89557, United States



ARTICLE INFO

Keywords:
 ABAQUS
 Direct pull test
 FE model
 Pipe pin
 Stud
 Tension
 Threaded rod

ABSTRACT

Base pipe pin connections were developed to simulate a hinge behavior at the base of cast-in-place or precast bridge columns. Base pipe pins are composed of two steel pipes: one pipe is embedded in the column and the other in the adjoining member. Shear force is transferred through contact of the pipes and friction. The uplift force is resisted by a tension member and welded studs on the surface of the column pipe. To investigate the behavior and failure mode of base pipe pins under direct tension and to determine the ultimate tensile capacity of the pins, two scaled pipe pin connections were tested under direct tension. Elaborate nonlinear finite element (FE) studies of the pipe pins were also conducted to explore the effects of different parameters on the response of the pins. There are many possible failure modes that could occur under tension. Test results depicted that rupture of the pin tension member with no damage to the connection was the dominant failure mode in pure tension. The FE models accurately estimated the response of the test models and the observed failure mode. The analytical results showed that decreasing the pipe height alters the failure mode but does not affect the ultimate capacity of the connection significantly. Furthermore, reducing the pipe height or increasing the number of stud layers has a small effect on the ultimate capacity and stiffness of the connections.

1. Introduction

Top pipe pin hinges were first developed by the California Department of Transportation (Caltrans) engineers to eliminate moment transfer between column and cap beam in cast-in-place (CIP) construction. Pipe pins consist of a steel pipe that is anchored in the column and extended into a steel can inside the cap beam. This type of connection is designed to transfer (1) axial load through bearing of the cap beam on the column while no tension is transferred, (2) shear between the column and the cap beam through contact of the part of the pipe that is protruded and the can in the cap beam and friction at the column-cap beam interface, and (3) no moment from the column to the cap beam [1].

To investigate the seismic performance of the pipe pins and to develop a reliable design method, extensive analytical and experimental studies have been conducted. Five groups of experiments were conducted at the Large Scale Structural Laboratory at UNR: (1) and (2) quasi-static test of two 0.3 scale hinged cantilever columns under pure shear and combined flexure, shear, and axial loads to investigate overall response of the pipe pins [2], (3) static test of six 1:3.5 scale push-off specimens to formulate the bearing strength of concrete against steel pipes [3], (4) static pure shear test of six infill steel tubes to determine

the shear capacity and develop an empirical design equation for shear strength of the tubes [3], and (5) shake table test of a 1:5 scale two-column bridge bent model incorporating top pipe pins to validate the design method developed for the pins [1]. Top pipe pins were also incorporated in several research projects to provide details for use in accelerated bridge construction (ABC) including shake table test of a 0.3 scale precast two-column bridge bent [4], biaxial shake table test of a quarter-scale four-span bridge [5], and shake table test of a quarter-scale two-span deconstructible bridge [6].

A new generation of pipe pins for column bases was developed by Mehrsoroush and Saiidi [7] for use in CIP or precast bridges. To study the seismic performance and response of the base pipe pins and to develop a reliable design method for these connections, a one-third scale, two-column bridge bent model incorporating column-footing pipe pins was subjected to quasi-static cyclic loading until failure. Test results revealed that the proposed pipe pin was successful in resisting the column reactions even under high drift ratios and could satisfy the Caltrans seismic design criteria [8] requirements as a capacity protected member.

A modified version of the base pipe pins were also used by Mehraein and Saiidi [9] in shake table study of a 1:3.75 scale precast two-column bridge pier model to connect bridge columns to pile shafts.

* Corresponding author.

E-mail address: a.mehrsoroush@nevada.unr.edu (A. Mehrsoroush).

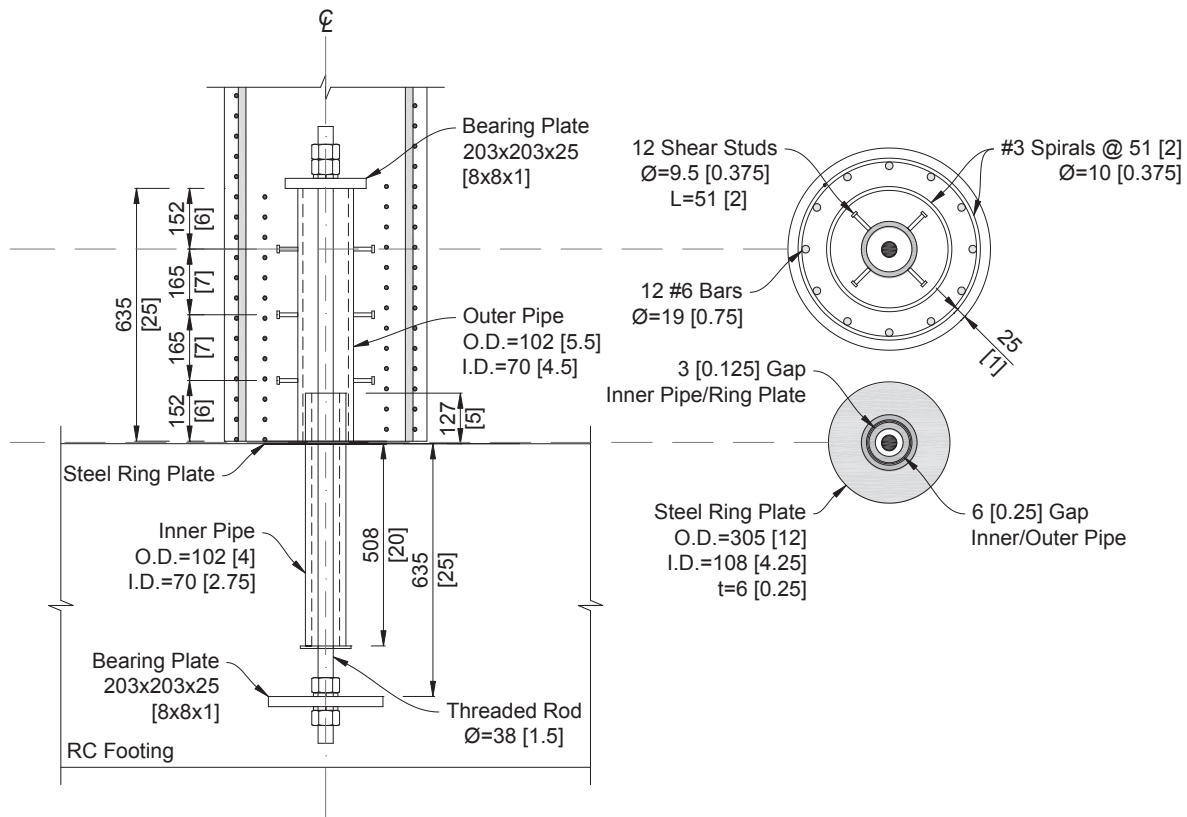


Fig. 1. Details of CIP-Col pipe pin connection (units: mm [in.]).

The study presented in this paper focuses on the tensile response of base pipe pins developed by Mehrsoroush and Saiidi [7]. The main objectives of the study were to determine (1) the ultimate behavior of base pipe pins under direct tension through experimental studies, and (2) the effects of different parameters on the response and failure mode of the pins under direct tension through nonlinear finite element studies of base pipe pin connections using ABAQUS [10]. The experimental studies were conducted on portions of the bent model that had been studied by Mehrsoroush and Saiidi [7].

2. Base pipe pin connection concept

Pipe pin connections are composed of two steel pipes (Fig. 1). One pipe is embedded in the column (referred to as the outer pipe hereafter) and the other is embedded in the footing (referred to as the inner pipe hereafter) and protrudes from the footing and extends into the outer pipe. An attempt was made initially to adopt the top pipe pin detail by using a steel pipe in the column and a can in the footing. However, this detail was not viable because base pipe pins are likely to undergo tension under overturning moments, whereas top pipe pins do not include a tension force transfer mechanism. Therefore, two steel pipes (as opposed to one pipe and one can in top pipe pins) were necessary to make the connection work. Shear between the column and the footing is transferred through direct contact between the pipes and friction at the column-footing interface. The tension resisting mechanism of pipe pins consists of (1) a high strength threaded rod passing through the pipes, (2) two plates at the ends of the rod anchored in the column and footing, and (3) welded studs on the surface of outer pipe to transfer the pipe force to concrete. The end plate in the column bears against the outer pipe and concrete while the plate in the footing is embedded in concrete. To enhance the rotational capacity of the hinge, the column is placed over a steel ring plate on the footing to form a hinge gap at column-footing interface. No reinforcing bars pass from the column to footing. The column compression is transferred to the footing through

bearing on the ring plate that is supported on the footing.

3. Experimental studies

3.1. Two-column bent model

A one-third scale two-column bent model was constructed comprising of a precast column, a conventional CIP reinforced concrete (RC) column, a precast cap beam, and two single footings. The columns were connected to the footings and cap beam using pipe pins and pocket connections developed by Mehrsoroush and Saiidi [7], respectively. Details of the two-column bent model are shown in Fig. 2. The clear height and span of the bent were 2540 mm (100 in.) and 3048 mm (120 in.), respectively. Both columns were 3150 mm (124 in.) in height and 508 mm (20 in.) in diameter with 12-#6 [bar diameter (db) = 19.1 mm (3/4 in.)] longitudinal bars providing a steel ratio of 1.68% and #3 [db = 9.5 mm (3/8 in.)] spiral at 50.8 mm (2 in.) pitch resulting in a volumetric transverse steel ratio of 1.25%. The precast column was designed to be used in ABC by utilizing two main segments: a 635-mm (25-in.)-high precast concrete pedestal, and an upper 2515-mm (99-in.)-high precast segment that incorporated engineered cementitious composite (ECC) and concrete. The longitudinal bars of the upper segment were extended below by 610 mm (24 in.) for subsequent insertion into the pedestal to provide a connection. The pedestal incorporated 12, 635-mm (25-in.)-high corrugated metal ducts aligned with the longitudinal bars of the upper segment and a #3 outer spiral at 50.8 mm (2 in.) pitch placed around the ducts. The corrugated ducts of the pedestal were filled with grout after insertion of the longitudinal bars from the upper segment. The precast column pipe pin was incorporated in the concrete pedestal using the same detail as the one for the CIP column. To enhance the shear capacity of the pipe pins, #3 inner spirals at 50.8 mm pitch (2 in.) and center-to-center diameter of 305 mm (12 in.) were placed around the outer pipes. Details of the pipe pins are depicted in Fig. 1.

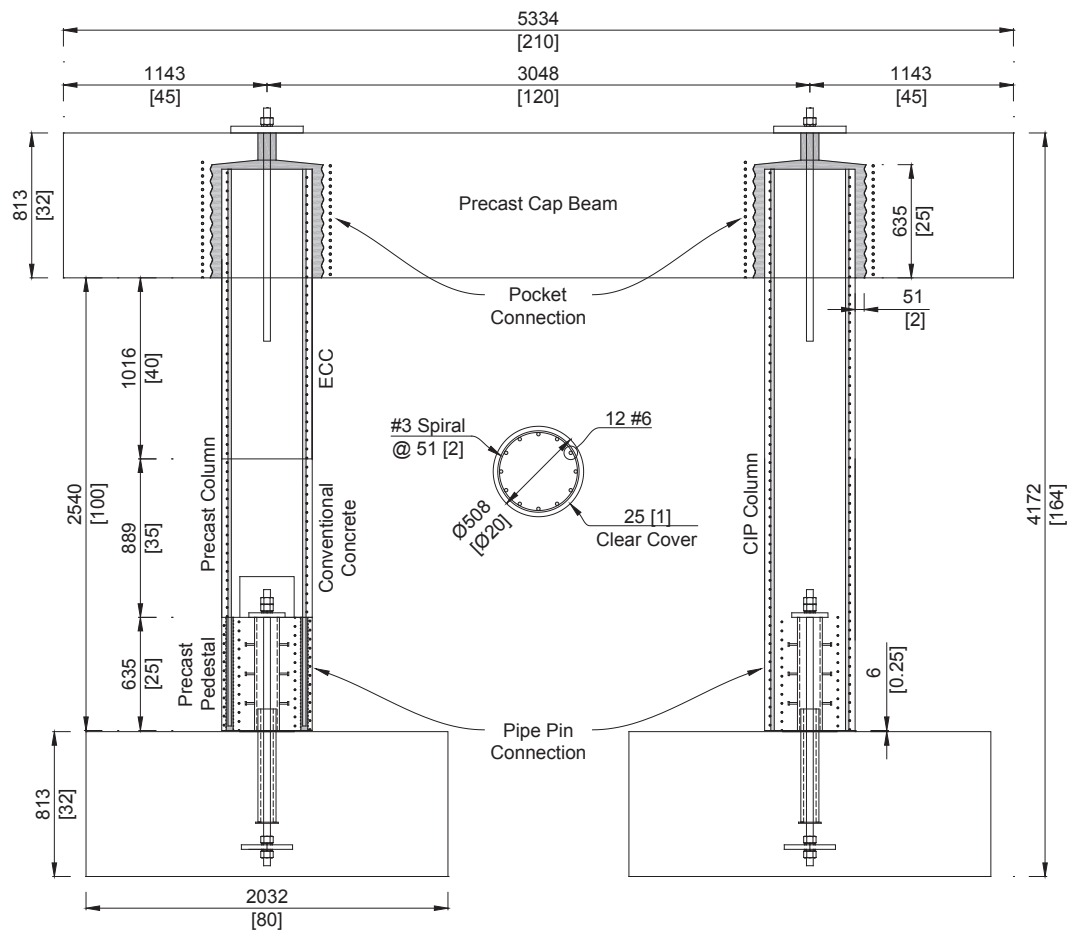


Fig. 2. Details of two-column bent model (units: mm [in.]).

3.2. Design of base pipe pin connections under tension

The study of the bent reported by Mehrsoroush and Saiidi [7] revealed an interesting behavior. As the pipe pin moved and rotated under lateral loading of the bent, the top bearing plate moved and rotated, an action that stretched the threaded rod even when the column was under compression. The resulting tension put the lower portion of the column within the pipe pin zone under compression even when the bent overturning moment resulted in tension in the column. Because tension member of the base pipe pins was always under tension, and subsequently the pipe within the column was always under compression, the tensile response of pipe pins was necessary to be studied.

The tension in the rod was the summation of the column uplift force and the force due to movement of the top end plate. The rod was also subjected to flexural moments due to movement of the top plate. The moment was estimated using the rod top head displacement and rotation when the hinge gap was fully closed and the pipes were in contact. The rod was designed for the maximum tension and moment. The tension in the rod was transferred to the end bearing plates causing the top plate to bear against concrete and the pipe and the bottom plate bear against the concrete. The bearing plates were designed to satisfy two limit states: (1) bearing strength of concrete and (2) flexural yielding of the plates. It was assumed that the pipe pin as a capacity protected member would remain elastic. Thus, the rod force at the top was distributed proportionally to the axial stiffness of concrete and the steel pipe. Neglecting the friction at the concrete-pipe interface, it was assumed that the entire compression of the outer pipe was transferred to the surrounding concrete through shear studs. The studs were designed based on the code requirements for shear strength of the studs [11] and the concrete pry out strength in shear [12]. The breakout

strength of concrete was not a governing limit state as the studs were embedded in a mass of reinforced concrete far from the free edges of the column. The footings were designed to be stiff and remain elastic under the cyclic loading tests of the two-column bent. The embedded depth of the bottom bearing plate in the footing was calculated so that the breakout failure of concrete [12] due to the rod tension is prevented. When the precast column underwent uplift forces, the tension was transferred to the pedestal through bond strength of longitudinal bars extended into the grouted metal ducts. The required development length of the ducts was calculated based on the results of previously conducted tests [13], accounting for the total number, material property, and configuration of the ducts.

Details of design of the columns, cap beam, and the pipes are presented in Mehrsoroush and Saiidi [14].

3.3. Construction and material properties

To construct the base pipe pins, the rods and bottom bearing plates were placed in the center of the footings bar cage and the inner pipes were positioned and secured in the footings at the specified height such that the rods passed through the centerline of each pipe (Fig. 3a). The footings were cast subsequently. The concrete pedestal was constructed in-place on top of the footing by placing the ring plate on top of the footing, placing the outer pipe over the ring plate around the inner pipe so that the rod passed through the pipe center line, placing the inner spiral, outer spiral, and corrugated metal ducts around the outer pipe, fixing the top bearing plate on top of the outer pipe, and casting the concrete (Fig. 3b). The concrete portion of the top precast segment was cast on a platform with the column longitudinal bars extended below the platform through pre-drilled holes. After curing, the top segment

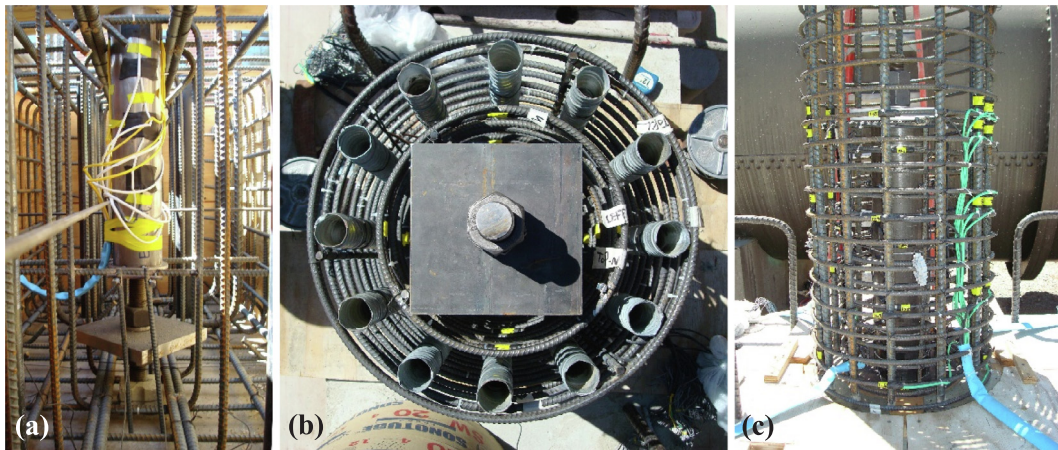


Fig. 3. Construction of pipe pins: (a) lower portion of pipe pins in footing; (b) precast column pipe pin; (c) CIP column pipe pin (images by Ali Mehrsoroush).

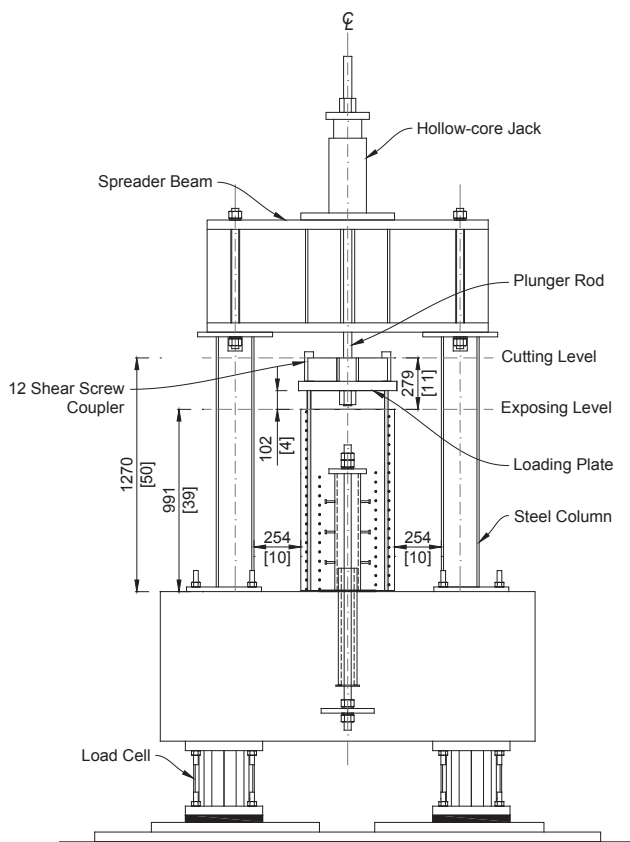


Fig. 4. Direct pull test setup details (units: mm [in.]).

was lowered onto the concrete pedestal while the extended bars were inserted into the grouted ducts to form the complete column. The pipe pin connection in the pedestal and CIP column had the same construction pattern except that only the inner spiral and column bar cage were placed around the outer pipe over the ring plate and the column was cast incorporating the pipe pin at the bottom (Fig. 3c).

Standard cylindrical samples of concrete, cubic samples of grout, and samples of the steel reinforcements were tested. The average measured test day compressive strength of the footings concrete, columns and pedestal concrete, and pedestal grout was 52.2, 45.6, and 74.0 MPa (7.57, 6.61, and 10.74 ksi), respectively. The average measured yield stress for the #3, #4, #6 reinforcing bars, and rods was 450.4, 533.4, 471.3, and 918.7 MPa (65.32, 77.36, 68.35, and 133.24 ksi), respectively. The yield strength of the steel for the inner pipes,

outer pipes, bearing plates, and shear studs was 581.9, 536.0, 295.1, and 430.9 MPa (84.4, 77.74, 42.83, and 62.5 ksi), respectively.

3.4. Preparation of pipe pin connection models for direct pull test

Among different options considered to apply the direct tension on pipe pins after the bent model cyclic testing, pulling the pins using the column longitudinal bars in a self-reacting loading frame was found to be the most appropriate. To prepare the pipe pins for the direct pull tests, the columns were saw cut at a height where the column longitudinal bars had not yielded during the cyclic loading test. The cutting level corresponding to the first yield moment of the column section was at 1270 mm (50 in.) above the footing top face. Cutting of columns was followed by exposing the column longitudinal bars for at least 279 mm (11 in.) to provide sufficient length to anchor the bars in the test setup. The test models were labeled PFPT and CFPT, which stand for precast footing pin tension test and cast-in-place footing pin tension test, respectively.

3.5. Instrumentation

To measure the load, displacements, and strains during the direct pull tests, 63 and 55 channels of data were collected in PFPT and CFPT, respectively. PFPT was instrumented using 22 longitudinal strain gauges at six levels on longitudinal bars, 16 strain gauges at six levels on outer spirals, 12 strain gauges at four levels on inner spirals, and eight longitudinal strain gauges on the outer pipe. Moreover, various aspects of CFPT response was monitored using 18 strain gauges at four levels, 24 strain gauges at three levels, and eight strain gauges at four levels on the longitudinal bars, inner and outer spirals, and outer pipe, respectively. The vertical displacement of the connections was measured by averaging the measurements of four displacement transducers in each model.

3.6. Test setup

Fig. 4 shows the schematic details for the direct pull test setup. The pipe pin connections were subjected to direct pull test using a loading plate and a self-reacting loading frame installed above the footings. The loading frame was composed of two steel columns, a spreader beam, and a hollow-core jack placed above the spreader beam. The column segments were placed symmetrically in-between the columns of the loading frame, and the longitudinal bars were anchored over a loading plate using shear-screw couplers. The loading plate was pulled up by the plunger rod of the hollow-core jack passed through the spreader beam and the loading plate central hole and was fixed under the plate. The tension of the jack was transferred uniformly from the loading plate



Fig. 5. Direct pull test setup for CFPT (image by Ali Mehrsoroush).

to the column segment longitudinal bars through the couplers. The complete direct pull test setup for CFPT is depicted in Fig. 5.

3.7. Loading protocol

The pipe pin connections were subjected to direct tension using a 890-kN (200-kips), 254-mm (± 10 -in.)-stroke hollow-core jack. The loading was initiated as load controlled and continued by increasing the

load amplitudes until the rods yielded. The target loads during the tensile loadings were 44.5, 133.4, 266.9, 400.3, 533.8, 667.2, and 800.7 kN (10, 30, 60, 90, 120, 150, and 180 kips), respectively. The loading was switched to displacement controlled at the onset of non-linearity in the pin force-displacement relationship. The displacement-controlled loading was initiated by increasing the total displacement to 20.3 mm (0.8 in.) after the rods began to yield and was continued by increasing the displacement amplitudes at 5.1 mm (0.2 in.) increments.

3.8. Test results

3.8.1. Apparent damage

Fig. 6a and b demonstrates the damage to PFPT and CFPT at 20.3 mm (0.8 in.) vertical displacement, respectively. No damage was observed in PFPT during the load-controlled portion of loading other than formation of minor tensile cracks on the top half of the concrete pedestal and separation of the column segment from the footing. By the end of the displacement-controlled portion of loading, the tensile cracks propagated over the height of the pedestal and the gap between the pedestal and the footing widened due to plastic deformations of the rod and the end bearing plates. The part of the column above the pedestal remained in contact with the pedestal during the test. After unloading, the pedestal rested on top of the ring plate because the top bearing plate was engaged only when the pedestal move upward and did not prevent the downward movement of the pedestal. The status of damage in CFPT at the end of the elastic and plastic portion of loading was the same as that of PFPT, except that a larger number of cracks propagated on the top half of the specimen. In contrast to PFPT, the top steel plate was embedded in concrete and restrained both upward and downward movement of the column. As a result, the base of the specimen did not bear on the ring plate upon unloading because the rod had yielded and there was some permanent deformation.

3.8.2. Post-test observations

The connection was disassembled after the test to inspect PFPT closely. It can be seen in Fig. 7a that the hex nuts had separated from the top bearing plate. This was due to the residual elongation of the rod and permanent bending of the end bearing plates (Fig. 7b). Permanent deformations of the tension member in reversal loadings cause a

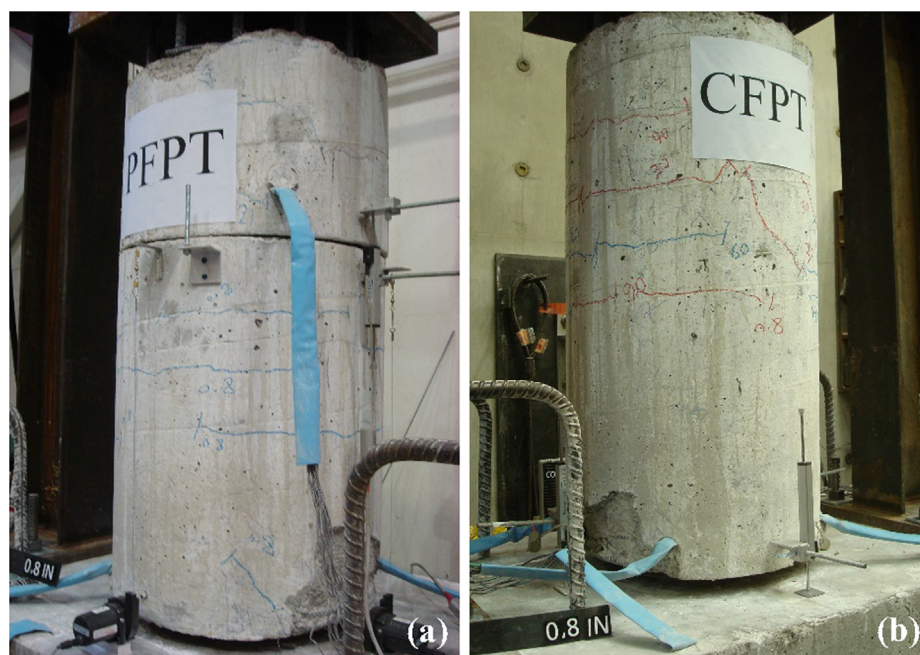


Fig. 6. Damage to pipe pin connections at 20.3 mm (0.8 in.) vertical displacement: (a) PFPT; (b) CFPT (images by Ali Mehrsoroush).

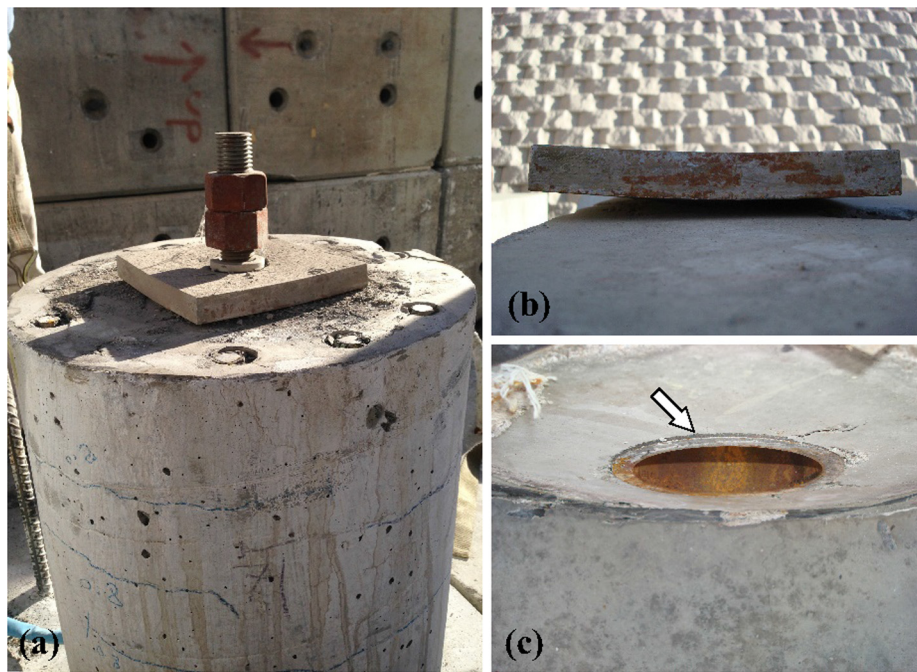


Fig. 7. Post-test status of damage to CFPT pipe pin components: (a) threaded rod; (b) top bearing plate; (c) outer pipe (images by ali Mehrsoroush).

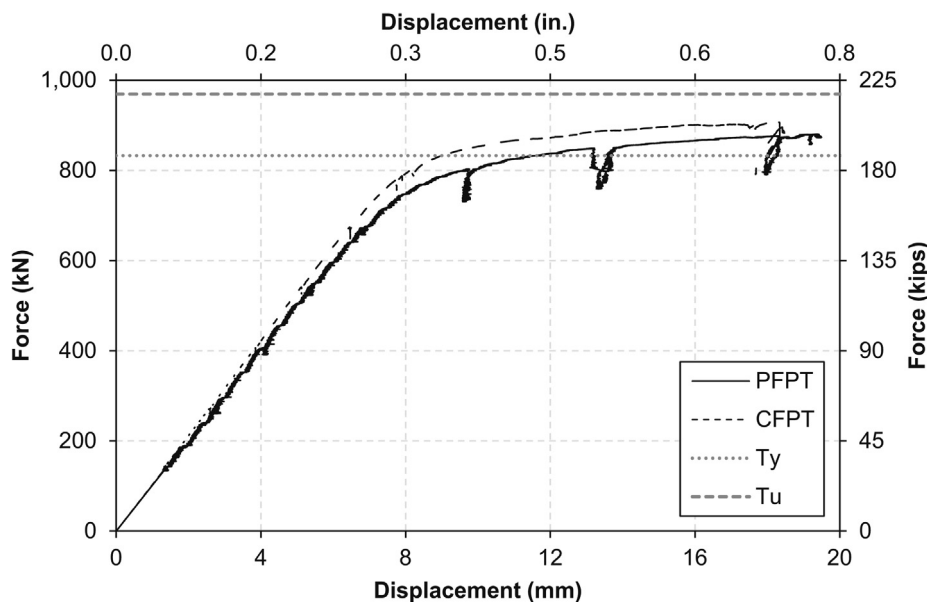


Fig. 8. Load-displacement relationship for pipe pins under direct pull tests.

progressive lag in development of tension in pipe pins, which needs to be prevented due to its detrimental effect on the overall performance of the connection. The outer pipe had slipped slightly out of the pedestal bottom face (Fig. 7c), indicating plastic deformation of shear studs in concrete. No sign of bearing failure was detected on the surface of the pedestal under the top bearing plate. The hex nuts also remained intact and no dethreading mark was noticed on the rod. The observations confirmed that (1) the tension of the rod was transferred to the pedestal, and (2) at initial loading steps, the tension was transferred through bearing of the top plate on the pedestal face and outer pipe cross section at the same time. By increasing the loading amplitude, the plate was bent and lost the contact with pedestal face. Subsequently, the load was transferred directly to the pipe through bearing of the plate on the pipe section.

3.8.3. Load-displacement relationships

According to Caltrans SDC [8], pipe pins need to be designed as capacity protected members and remain essentially elastic in seismic events. However, to investigate the behavior and response of connections, they were loaded to failure in the present study. The measured axial load-displacement response for PFPT and CFPT is shown in Fig. 8. Ty and Tu in this figure represent the yield and ultimate tensile capacities of the rod, respectively, determined using uniaxial tensile test of rod samples. The connections underwent some displacements under minimal load during the early stages of loading before the couplers were set. The diagrams were offset to delete those portions of the curves.

The force-displacement response of the pins exhibited the same trend as that of rod samples tested under uniaxial loading. However, pipe pins showed softer response because the load path involved several

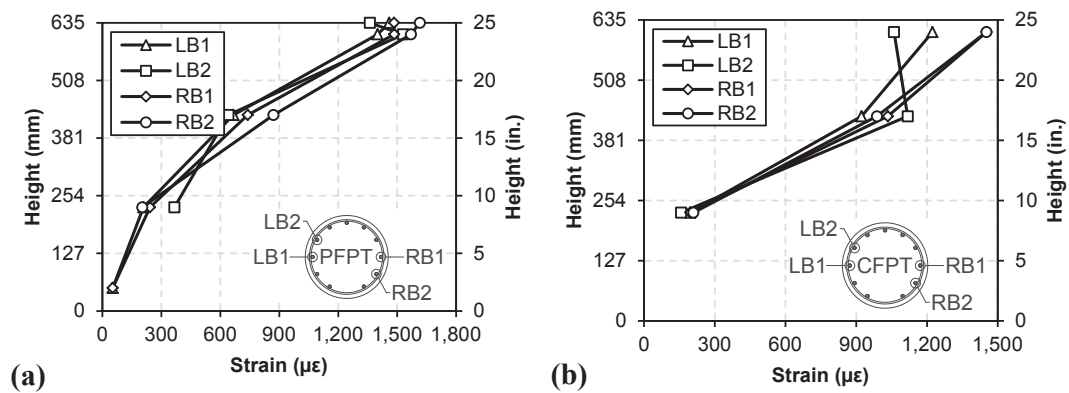


Fig. 9. Peak strain profiles of longitudinal bars: (a) PFPT; (b) CFPT.

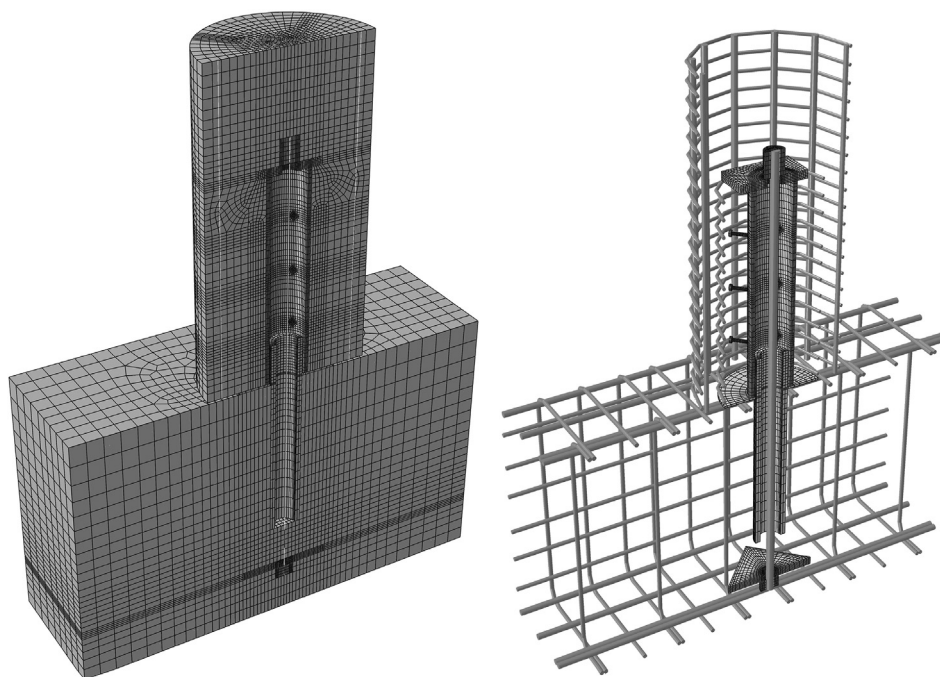


Fig. 10. Details of CFPT FE model and reinforcements.

components such as the studs and the end plates and these components introduced flexibility in the system. The initial stiffness of the connections was 99.1 kN/mm (565.6 kips/in.) for PFPT and 104.7 kN/mm (597.7 kips/in.) for CFPT. PFPT was slightly softer due to segmental construction. Both specimens were tested under tensile loading until the full capacity of the jack was reached. Substantial yielding occurred but the rods did not fracture. The maximum achieved tensile capacity for PFPT and CFPT was 880.3 and 907 kN (197.9 and 203.9 kips), obtained at 19.3 and 18.3 mm (0.76 and 0.72 in.) displacements, respectively. The measured ultimate capacity of the rods was 969.3 kN (217.9 kips).

3.8.4. Strain data

The maximum tensile strains in the column longitudinal bars of PFPT and CFPT were 1615 and 1583 µε, respectively, measured at 635 and 660 mm (25 and 26 in.) above the column base. These strains were less than the yield strain of 2357 µε and indicated that the displacements in Fig. 8 were not affected significantly by deformation within the column. Comparison between the peak measured strains in the column longitudinal bars (Fig. 9) showed that the test setup was successful in achieving uniform distribution of the force among the longitudinal bars and eliminated any moment that might act on the test model.

The inner and outer spirals reached the maximum strains of 59 and 81 µε for PFPT and 56 and 384 µε for CFPT, respectively. The peak measured strains in both spirals were far below the yield strain of 1662 µε, indicating that neither spirals played a role in the test.

The outer pipe force was transferred to the surrounding concrete through the shear studs on the pipe surface and shear transfer at pipe-concrete interface through friction. Consequently, the pipe was subjected to compression up to the bottom row of the studs. PFPT and CFPT outer pipes reached the maximum compressive strain of -301 and -137 µε, recorded at 324 mm (12.75 in.) above the column bottom face. The outer pipes in both connections remained elastic during the entire testing since the maximum measured strains were much less than the yield strain of 2681 µε. All the peak measured strains occurred at 30.5 and 25.4 mm (1.2 and 1.0 in.) vertical displacements in PFPT and CFPT, respectively.

The measured strains and post-test observations indicated that the plastic deformations of the rod, studs, and bearing plates are the main sources of nonlinearity in the response of pipe pins to direct tension.

4. Analytical studies

Analytical studies of the test models were conducted to verify the

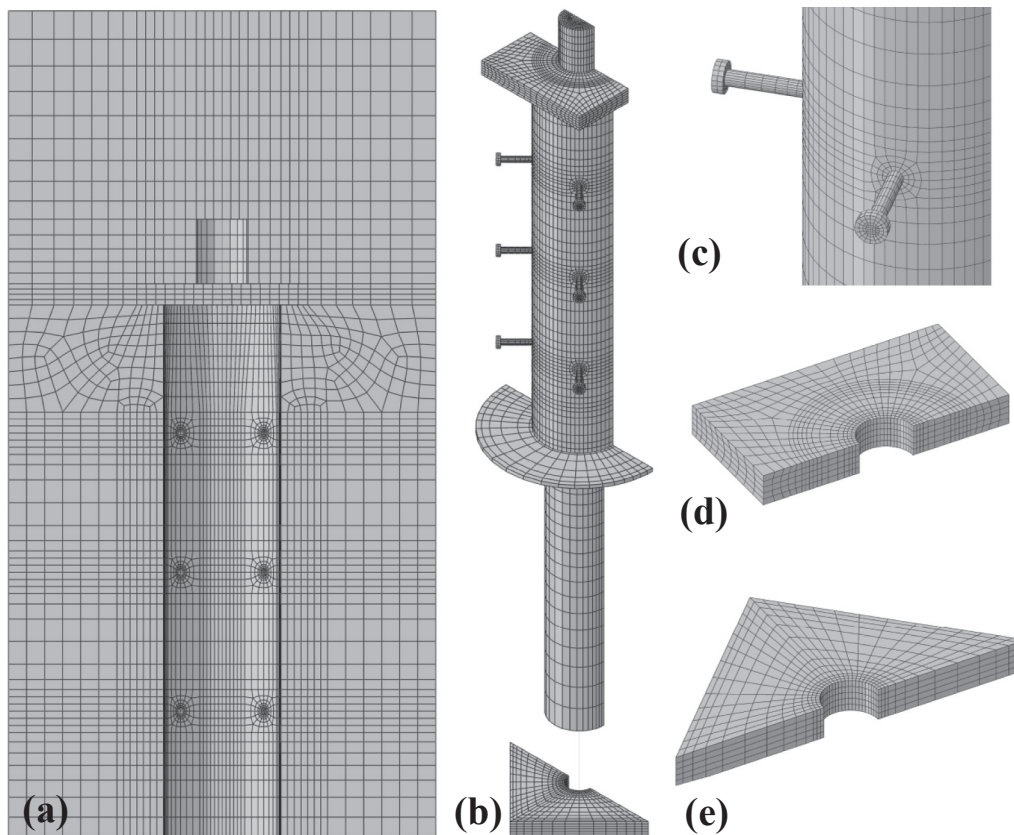


Fig. 11. FE mesh of CFPT components: (a) concrete column segment; (b) steel parts; (c) shear studs; (d) top bearing plate; (e) bottom bearing plate.

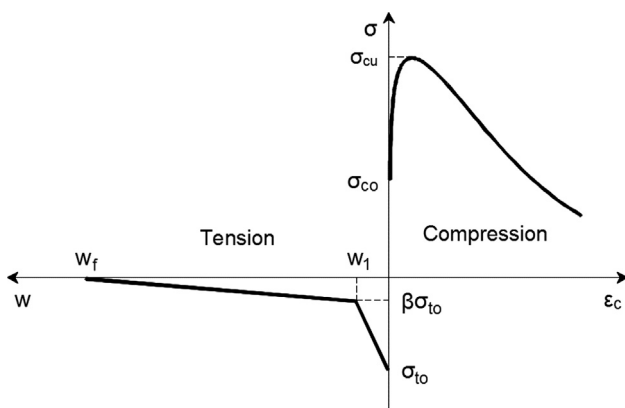


Fig. 12. Uniaxial stress-plastic deformation relationship for concrete.

validity of the modeling assumptions by test data and develop a reference model for further studies. To understand and quantify the effects of key parameters on the behavior, capacity, and failure mode of pipe pins, a comprehensive parametric study was conducted using the validated FE model.

4.1. Model details

A detailed nonlinear FE model of the pipe pin connections was developed, and the results were compared with the test data. The finite element program ABAQUS/Explicit v6.11 package was utilized because of its capabilities and features for modeling materials and interactions. This software has been utilized by other researchers in several related studies including the study of bearing strength of concrete against steel pipes [3], the force transfer mechanism in concrete-filled steel tubes [15], and behavior of headed stud shear connectors in composite beams [16].

Due to geometric symmetry of the pipe pins and symmetry of the loading, only one-half of the test models were simulated. All the solid elements were modeled using reduced integration first-order hexahedral (brick) elements (C3D8R). The reduced integration elements were used to avoid excessive computer run time and maintain a balance between computational efficiency and accuracy. Reinforcing bars of the footing and longitudinal bars of the column were modeled using 3-node quadratic beam elements (B32), which is able to capture flexural and axial deformations. This is different than the common modeling of reinforcement in flexural members in which the bars are modeled as axial members only. Using B32, any local flexural deformation of the bars could be captured. Column spirals were modeled using 2-node linear 3-D truss elements (T3D2). The mesh sizes were refined around the contact surfaces to minimize the mesh distortion. Because the third root

Table 1
Modeling parameters for concrete damage plasticity.

	σ_{co} (MPa)	σ_{cu} (MPa)	E_c (MPa)	K_c	ϵ	σ_{to}/σ_{co}	ν_c	ψ	σ_{to} (MPa)	β	w_1 (mm)	w_f (mm)
Column	20.52	45.66	31,768	0.67	0.1	1.16	0.15	37	3.76	0.25	0.02	0.184
Footing	23.50	52.28	34,077	0.67	0.1	1.16	0.15	37	4.02	0.25	0.02	0.183

Note: 1 ksi = 6.895 MPa; 1 in. = 25.4 mm.

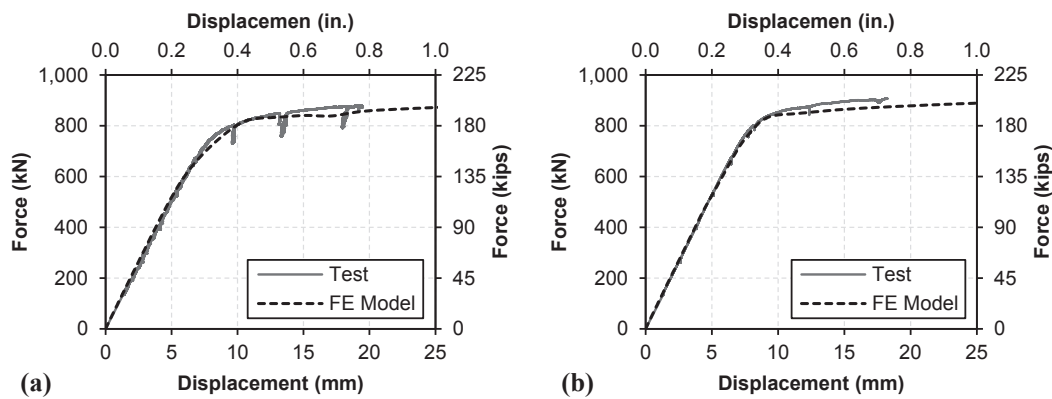


Fig. 13. Test vs. FE model load-displacement relationship: (a) PFPT; (b) CFPT.

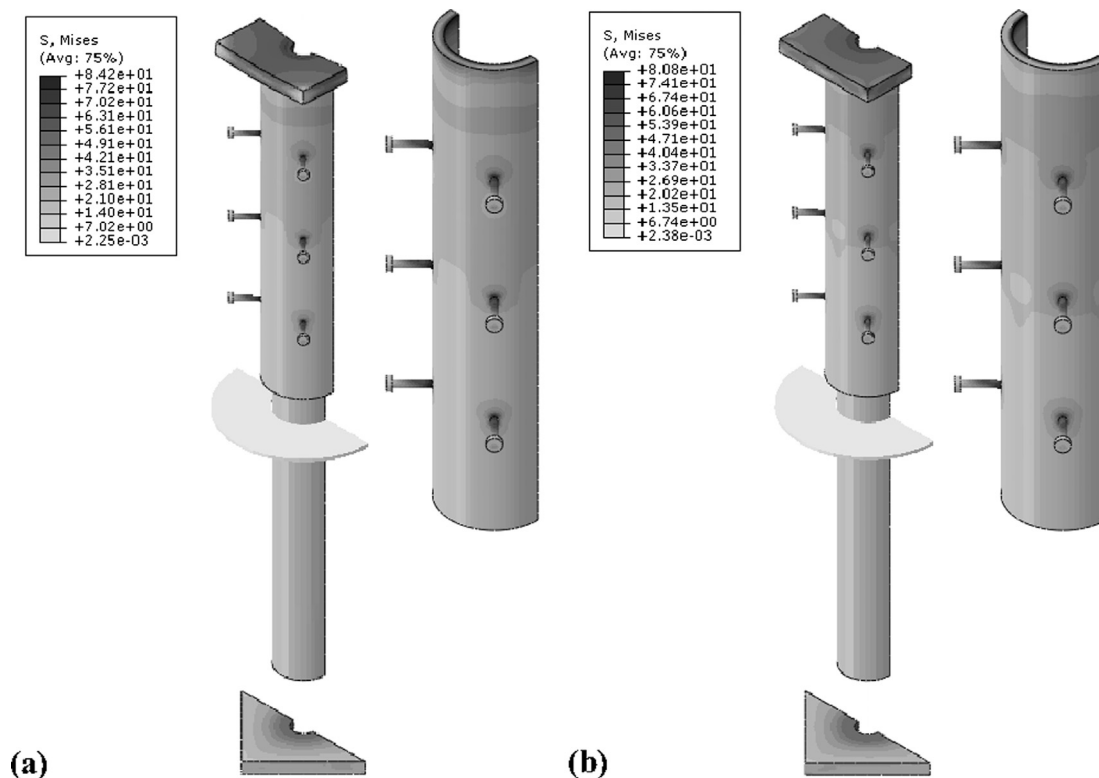


Fig. 14. Von Mises stresses (S): (a) PFPT; (b) CFPT.

of the element volume controls the tensile characteristic of concrete elements, flat or narrow concrete elements were not used in critical regions of the models.

Fig. 10 shows the details of FE model and reinforcements of CFPT. The FE mesh for CFPT components is depicted in Fig. 11. The FE modeling of PFPT was similar to CFPT, except for the concrete column segment. Overall, more than 72,700 and 74,100 elements were used for the simulation of PFPT and CFPT under direct pull tests, respectively.

Concrete damage plasticity model (CDP) was used to model the concrete parts. This model provides a general capability for analysis of concrete structures under monotonic, cyclic, and dynamic loading when the confining pressure of concrete is less than five times the concrete uniaxial compressive strength. The concrete failure mechanisms in the CDP model are characterized by tensile cracking and compressive crushing of concrete. The CDP uses concepts of isotropic damaged elasticity in combination with isotropic tensile and compressive plasticity to represent the inelastic behavior of concrete [10]. This model assumes that the uniaxial tensile and compressive response of

concrete are identified by damaged plasticity. The stress-strain relationship of concrete in the elastic region was defined by the modulus of elasticity. The post-elastic response of concrete under tension and compression was defined as the crack width and compressive inelastic strain versus concrete stress, respectively (Fig. 12). Because the displacement across a crack in a concrete section should be independent of the mesh sizing, the stress-displacement relationship was used to model the tensile behavior of concrete. The fracture energy concept proposed by Hillerborg et al. [17] was utilized to characterize the nonlinear behavior of concrete as a stress-displacement response. The uniaxial compressive stress-strain relationship of concrete was determined using the model proposed by Popovics [18]. The CDP model uses a yield condition incorporating different evolution of strength under tension and compression. The evolution of the yield (or failure) surface is controlled by two hardening variables, tensile and compressive equivalent plastic strains. The parameters listed in Table 1 were used to model the concrete in the column and footing. In this table, E_c , K_c , ϵ , σ_{bo}/σ_{co} , ν_c , and ψ are the parameters used to define the yield function

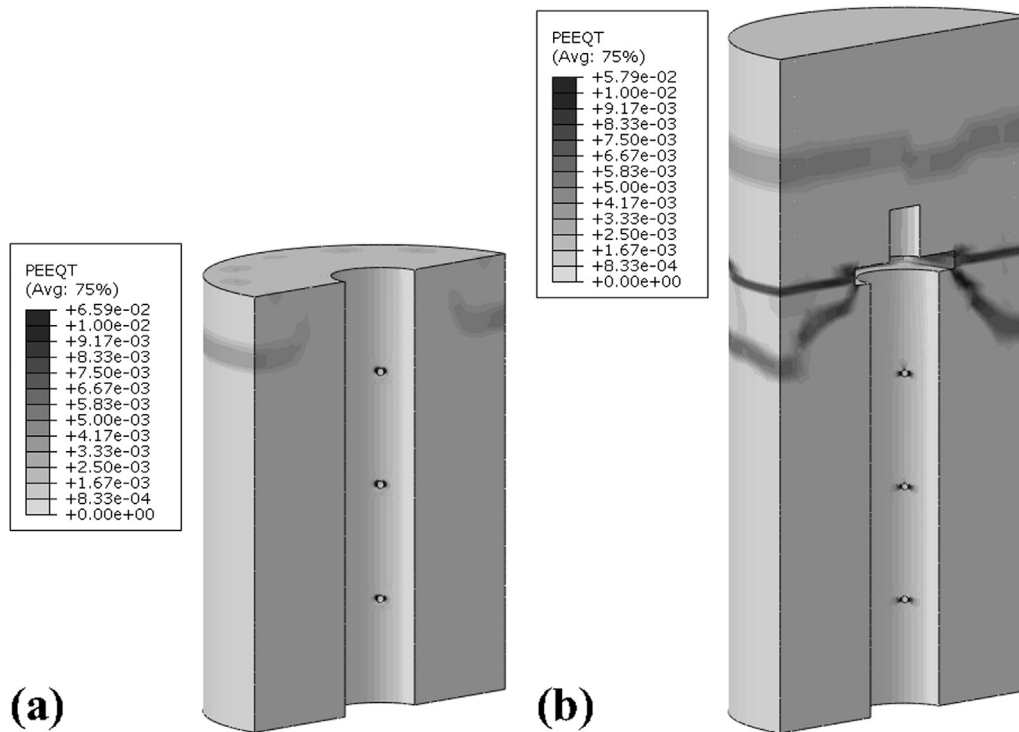


Fig. 15. Tensile damage (PEEQT): (a) PFPT; (b) CFPT.

and potential plastic flow of CDP model. The other parameters of the table are defined in Fig. 12.

The classical metal plasticity model was used to define the material property of the steel parts. The isotropic yielding was defined using the standard Mises yield surfaces with associated plastic flow. For longitudinal bars and rods, the complete stress-strain relationship obtained from uniaxial tensile tests was used. However, due to a lack of test data, Ramberg-Osgood model [19] was used to define the strain-stress relationship of the steel parts. The nominal stress-strain relationships representing the post-elastic behavior of steel parts were converted to true stress-plastic strain relationships as ABAQUS inputs.

Interaction between the elements was modeled using “Contact Pairs” algorithm. The interacting contact surfaces were specified separately as master and slave surfaces. “Hard” and “Penalty” mechanical properties were assigned to the contact surfaces in the normal and tangential directions, respectively. The hard contact relationship assumes a zero stiffness once the interface surfaces separate and an infinite stiffness once the gap between them is recovered. The tangential interaction of contacting surfaces was defined using linear Coulomb friction model. The basic concept of this model correlates slippage to the maximum critical shear stress between the contact surfaces using a coefficient of friction. Results of the parametric studies conducted on pipe pin subjected to lateral loadings indicated that the linear Coulomb friction model can sufficiently predict the tangential interactions [14]. The coefficient of friction for steel on steel, steel on concrete, and concrete on concrete was assumed to be 0.3 [20], 0.45 [21,22], and 0.45 [23], respectively. The friction coefficient for concrete on concrete accounts for degradation of stiffness due to cyclic action that the test models had undergone in the test bent model. Contact between the parts subjected to high normal compression (e.g. top bearing plate and outer pipe) was defined using contact pairs algorithm with kinematic method to override any penetration of elements at contact interfaces.

The ABAQUS “Standard” packager has convergence difficulties in problems with large number of iterations and complex materials. Therefore, “Explicit” packager was utilized to capture complicated three-dimensional contacts with concrete nonlinearities.

The embedded element technique was utilized to define the

reinforcing bars in 3D-solid concrete elements. The pipe pin connections were subjected to displacement-controlled loading through a reference node on the centerline of the models constrained to the longitudinal bars top nodes using rigid body tie constraints. To reduce the dynamic effects resulting from sudden application of the loads to the model, the loading was applied in a smooth manner using a smooth-step amplitude curve.

4.2. Results of FE analysis

Fig. 13 compares the test and FE analysis load-displacement relationships for PFPT and CFPT. The analytical models were successful in estimating the elastic stiffness, softening, post-elastic stiffness, and ultimate capacity of the connections under pure tension. Sample field outputs of the models at 64 mm (2.5 in.) displacement are presented in Figs. 14 and 15. Fig. 14a and b depict the Von Mises stresses (S) on the steel parts of PFPT and CFPT, respectively. The tension of the rod caused the top bearing plate of PFPT to bend in the middle and separate from the top face of the pedestal. Consequently, the tension was transferred directly to the outer pipe through bearing on top of the pipe (Fig. 14a). The curvature of the plate caused the contact force to be transferred to the inner edge of the pipe top section (edge contact). Because the top bearing plate of CFPT was embedded in the concrete, bending of the plate was resisted by the surrounding concrete resulting a smaller tension to be transferred to the pipe compared to PFPT. The Von Mises stresses on the shear studs indicate that concrete and studs were subjected to high contact pressures close to outer pipes. The high concentrated stresses on the top surface of the studs at the point of connection to the pipes resulted in the studs shear deformation (kinking). Distribution of Von Mises stresses over the outer pipe height shows that contribution of the studs in transferring the pipe load to concrete decreased as the distance from the top bearing plate was increased. The results also showed that the outer pipes underwent a high compressive axial force in between the top plate and the lowermost layer of the studs. The magnitude of this force decreased as the distance from the top plate was increased due to transfer of the force from the studs to concrete. It was assumed that concrete cracking initiates at

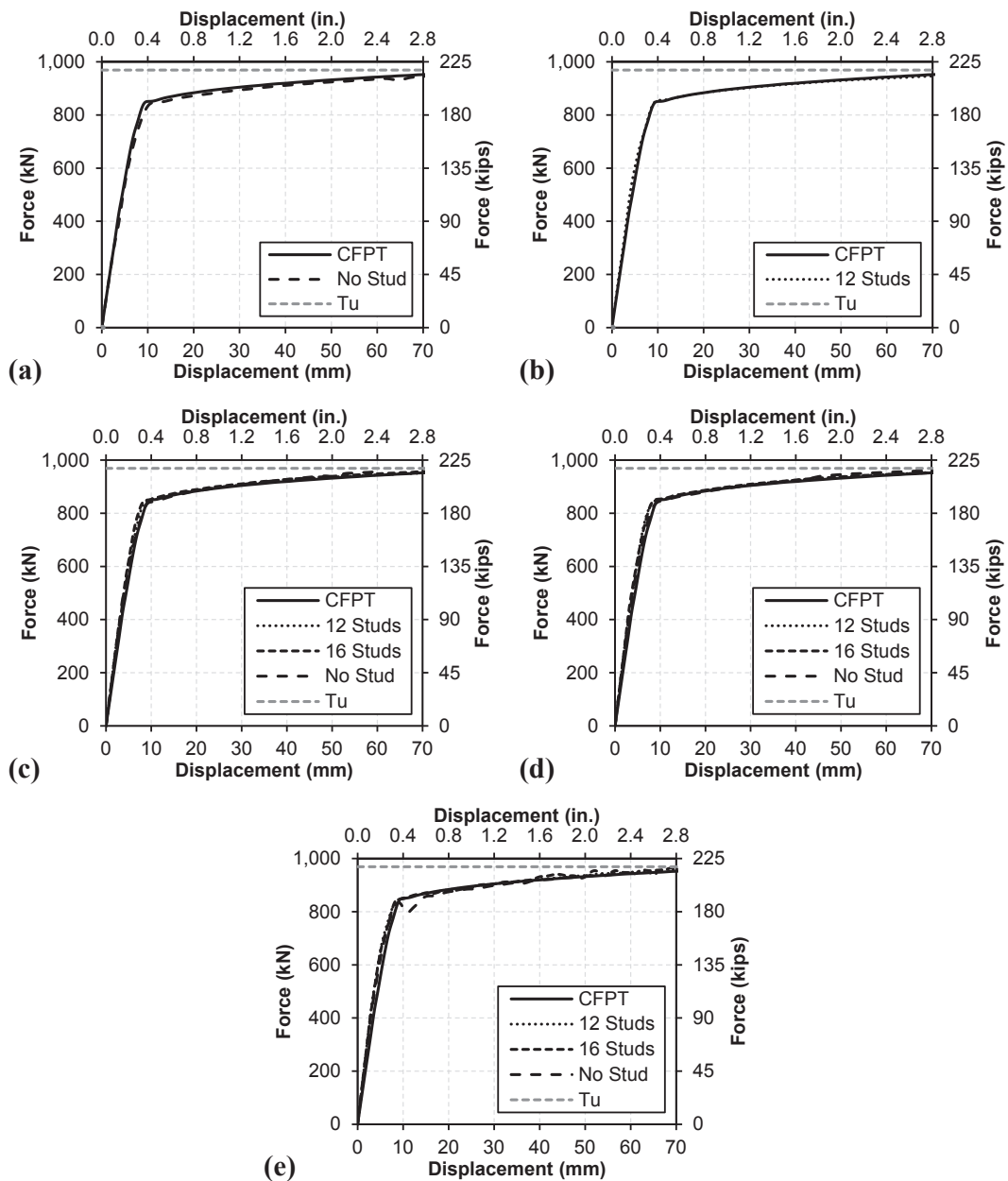


Fig. 16. Effect of number of studs on force-displacement response of pipe pin connection under direct tension: (a) Hop = 0.25Hc; (b) Hop = 0.2Hc; (c) Hop = 0.16Hc; (d) Hop = 0.14Hc; (e) Hop = 0.12Hc.

points where the tensile equivalent plastic strain (PEEQT) is greater than zero. PEEQT is a measure of the crack width, as the tensile behavior of concrete is defined in terms of stress-displacement [10]. The pattern of tensile damage for PFPT and CFPT concrete at 64 mm (2.5 in.) displacement is shown in Fig. 15a and b, respectively. A conical cracking was formed in CFPT (Fig. 15b) as a result of (1) normal compression transferred to concrete from the top corners of the bearing plate, and (2) change in the load transfer mechanism at the top bearing plate. The concrete body of the connection over the bearing plate was subjected to pure tension, whereas it underwent high compression below the bearing plate close to the pipe and tensile forces at location of the column longitudinal bars. The load was transferred between the longitudinal bars and the outer pipe (shear studs and top bearing plate) through compressive struts. The conical crack was formed over the uppermost compressive strut where the concrete was subjected to tension. The tensile cracking in the concrete pedestal of PFPT was limited to location of the shear studs and longitudinal bars, which extended

over a short depth from the concrete surface (Fig. 15a). The conical crack pattern was not observed in PFPT due to the absence of concrete over the top bearing plate.

5. Parametric studies

The parametric studies were conducted to investigate the effects of outer pipe height and the number of stud layers on the tensile performance and response of pipe pins. The CFPT FE model was utilized to perform the parametric studies because it was verified against the test data indicating its reliability.

5.1. Details of models

Changing the outer pipe height might change the capacity and dominant failure mode of the connection under tension. The pipe height (Hop) was reduced as a percentage of the column clear height (Hc)

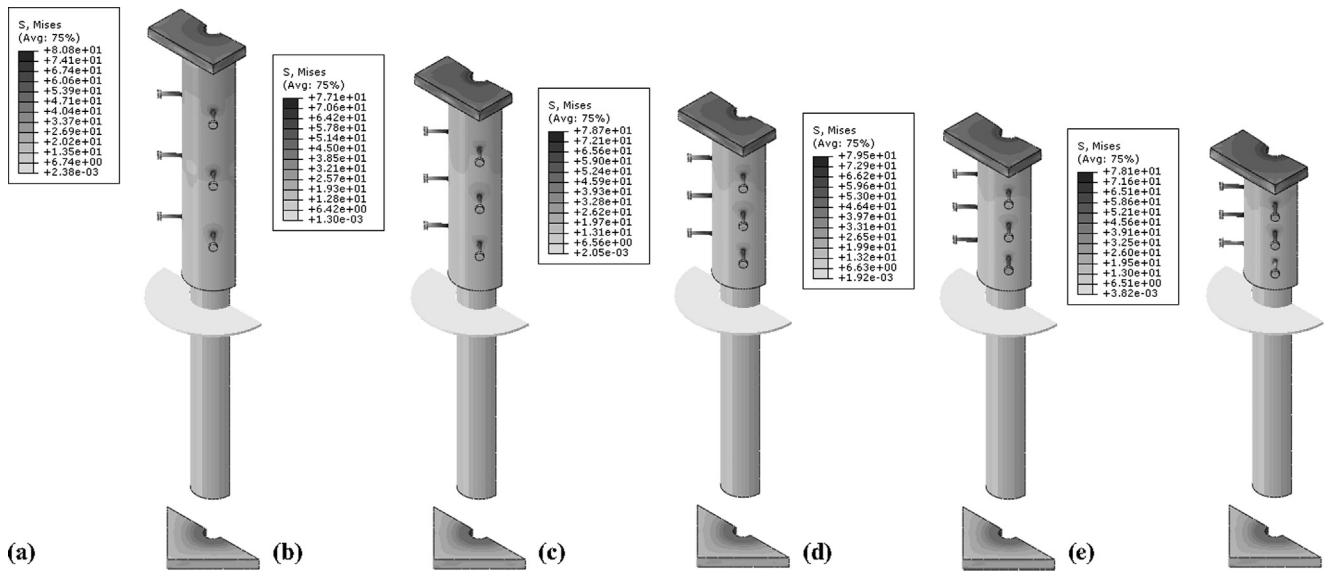


Fig. 17. Von Mises stress (S) variation: (a) Hop = 0.25Hc; (b) Hop = 0.2Hc; (c) Hop = 0.16Hc; (d) Hop = 0.14Hc; (e) Hop = 0.12Hc.

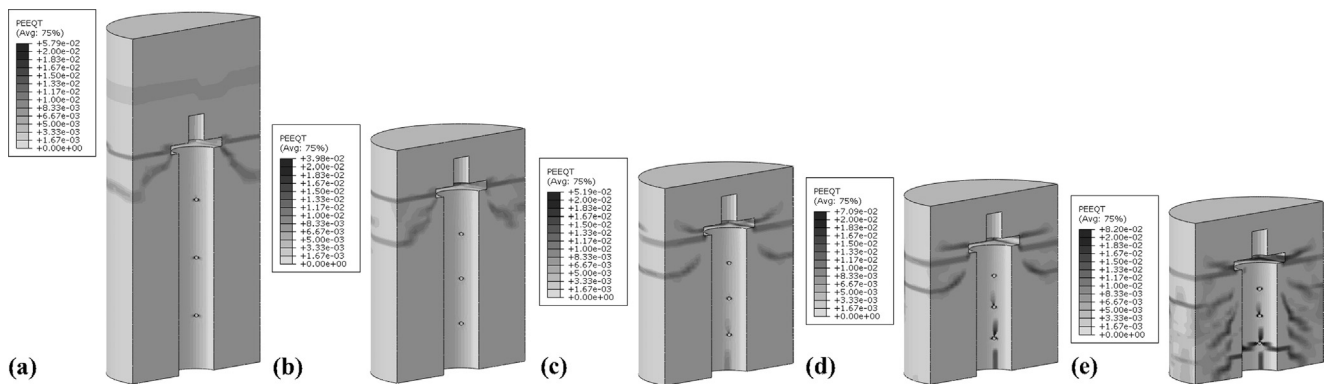


Fig. 18. Tensile damage (PEEQT) variation: (a) Hop = 0.25Hc; (b) Hop = 0.2Hc; (c) Hop = 0.16Hc; (d) Hop = 0.14Hc; (e) Hop = 0.12Hc.

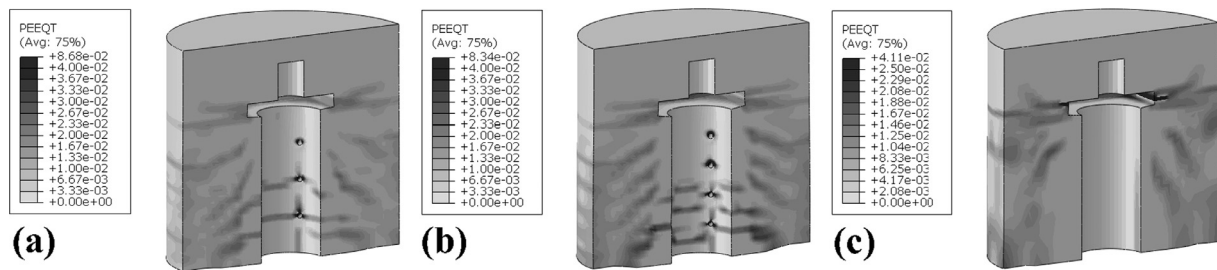


Fig. 19. Tensile damage (PEEQT) for Hop = 0.12Hc: (a) three stud layers; (b) four stud layers; (c) no stud.

(25%, 20%, 16%, 14%, and 12%) and different number of shear studs (zero, three, and four stud layers) with equal vertical spacing (0.25Hop and 0.2Hop, respectively) were included in the modeling of each case. Four studs spaced equally around the perimeter of the pipe were used at each layer. Four layers of stud were only incorporated in models with shorter pipes (Hop = 0.16, 0.14, and 0.12Hc) to study the effect of interfering compressive struts formed between the studs and perimeter rebars on the failure mode and capacity of pipe pins. Except for the connection with Hop = 0.25Hc (CFPT) replicating the test model, in all other cases the top bearing plate was embedded in concrete and the connection was modeled to 127 mm (5 in.) above the top face of the top bearing plate. Details of the FE modeling of the connections were the same as those of CFPT. The CFPT FE model (Hop = 0.25Hc with 12 studs) was selected as the reference model.

5.2. Results of FE analysis

The results of the parametric studies helped gain insight on the effect of different variables in the course of development of design recommendations presented in Section 6. Fig. 16 shows the sensitivity of the load-displacement response to the number of the studs and height of the outer pipe. The ultimate capacity and load-displacement response of the connections with the same Hop and different stud pattern did not vary significantly with the number of the studs. An increase in the number of studs slightly increased the initial stiffness of the response, but did not affect the ultimate capacity. This occurred because the pipe force was distributed among more studs resulting in smaller shear and flexural deformations of the studs, hence smaller bearing pressures on concrete at location of the studs. Models without stud showed a slightly

smaller initial stiffness compared to the models with studs; however, the ultimate capacity was not affected. Decreasing the pipe height altered the failure mode from the rod rupture for Hop = 0.25Hc to 0.14Hc to concrete failure for Hop = 0.12Hc (Fig. 18) but did not have a significant effect on the initial stiffness, ultimate capacity, and ductility of the connections compared to the reference model (Fig. 16). Contrary to expectation, tensile capacity and stiffness corresponding to concrete failure for Hop = 0.12Hc differed slightly from those corresponding to rod rupture for other cases. This occurred because change of the pipe height was not enough to let the concrete failure cause a significant effect on the capacity and stiffness.

The variation of Von Mises stresses on the steel parts and tensile damage in the concrete pedestal at 64 mm (2.5 in.) vertical displacement for models with three layers of stud is depicted in Figs. 17 and 18, respectively. The contribution of the studs to resisting the pipe force was smaller for the studs with farther distance from the top bearing plate. Part of the rod axial force was transferred to concrete through bearing of the top plate on concrete. Contribution of concrete in resisting the rod tension was proportional to the axial stiffness of the pipe, the axial stiffness of concrete, and the flexural stiffness of the bearing plate. Under high axial forces, bearing of the plate on concrete was diminished as a result of the plate bending. These contact pressures were the highest in models without stud and were reduced by increasing the number of studs. The top bearing plate underwent extensive curvatures in the models without stud. Under high axial forces, pipe slipped, and thus the bearing stresses shifted away from center onto concrete resulting in the higher flexural moments in the plate. Presence of the shear studs increased the axial stiffness of the pipe, thus decreasing the curvature in the plate. These observations were similar in all the analyses and indicate that in models with studs, pipe can be conservatively designed for the full axial force of the tension member.

Formation of a conical crack originating from the top bearing plate and extending toward the connection surface was the dominant failure mode of concrete in models with different pipe heights regardless of the number of studs (Fig. 18). In the models without stud, the cracks were more extensive and steeper toward the bottom than the ones with studs, and the angle of inclination of the crack increased by decreasing the pipe height. The same tendency was not observed in models with studs. The crack pattern in models with three and four layers of stud was nearly similar and was not significantly affected by the pipe height. As a sample, the effect of various numbers of stud layers on the crack pattern of models with Hop = 0.12Hc is depicted in Fig. 19.

The dominant failure mode in models with Hop = 0.12Hc was failure of concrete in tension resulting in the slip of the pipe and its surrounding concrete out of the connection (Fig. 18e). The inner and outer spirals did not contribute to the capacity of concrete because they did not pass through the failure plane.

6. Conclusions

The experimental and analytical studies presented in this article demonstrated that precast and CIP pipe pin connections developed in this study are able to undergo tensile loads exceeding the yield force of the tension members. Based on the measured strain data and test observations, the rupture of the rod is the most likely mode of failure for base pipe pins under pure tension.

Result of the FE nonlinear modeling illustrated that the experimental response could be accurately estimated in terms of the elastic stiffness, softening, post-elastic stiffness, and ultimate capacity of the connections under pure tension when a proper FE solver, material constitutive models, contact algorithms, and element models are used.

The parametric studies revealed that under direct tensile forces reducing the pipe length to 12% of the column height or increasing the

number of stud layers beyond the strength requirements has a small effect on the load-displacement response, ultimate capacity, and displacement ductility of pipe pin connections. However, the dominant failure mode changes from rupture of the rod for Hop = 0.25Hc to 0.14Hc to concrete failure and pipe pullout for Hop = 0.12Hc.

Acknowledgement

The study presented in this paper was funded by Caltrans under grant No. 65A0423. The writers are grateful for the support and assistance from Mr. Peter Lee and Dr. Amir Malek of Caltrans. Also assistance from Drs. P. Laplace, M. Tazarv, M. Mehraein, and A. Zaghi and Messrs. C. Lyttle, M. Lattin, and B. Nakashoji is highly appreciated.

References

- [1] Zaghi AE, Saiidi SM, El-Azazy S. Shake table studies of a concrete bridge pier utilizing pipe-pin two-way hinges. *J Bridge Eng* 2010;16(5):587–96.
- [2] Doyle KA, Saiidi M. Seismic response of telescopic pipe-pin connections [Report no CCEER-08-01]. Reno (NV): Center for Civil Engineering Earthquake Research, Department of Civil and Environmental Engineering, University of Nevada, Reno; 2008.
- [3] Zaghi AE, Saiidi MS. Bearing and shear failure of pipe-pin hinges subjected to earthquakes. *J Bridge Eng* 2010;16(3):340–50.
- [4] Motaref S, Saiidi MS, Sanders D, Mirmiran A. Shake table studies of a precast bridge pier with advanced materials. *Int J Bridge Eng* 2016;135–62 [special issue].
- [5] Kavianipour F, Saiidi M. Shake table testing of a quarter-scale 4-span bridge with composite piers [Report no CCEER-13-17]. Reno (NV): Center for Civil Engineering Earthquake Research, Department of Civil and Environmental Engineering, University of Nevada, Reno; 2013.
- [6] Varela S, Saiidi MS. Experimental study on seismically resilient two-span bridge models designed for disassembly. *J Earthquake Eng* 2019;23(1):72–111.
- [7] Mehrsoroush A, Saiidi MS. Cyclic response of precast bridge piers with novel column-base pipe pins and pocket cap beam connections. *J Bridge Eng* 2016;21(4):04015080.
- [8] Caltrans seismic design criteria (SDC). Sacramento (CA): California Department of Transportation; 2013.
- [9] Mehraein M, Saiidi M. Seismic performance of bridge column-pile-shaft pin connections for application in accelerated bridge construction [Report no CCEER-16-01]. Reno (NV): Center for Civil Engineering Earthquake Research, Department of Civil and Environmental Engineering, University of Nevada, Reno; 2016.
- [10] Hibbitt, Karlsson, & Sorensen Inc. ABAQUS/explicit user's manual. Version 6.11, vols. I and II. Pawtucket (RI); 2011.
- [11] AASHTO. AASHTO LRFD bridge design specifications. Washington, DC: American Association of State Highway and Transportation Officials; 2012.
- [12] ACI 318. Building code requirements for reinforced concrete. Detroit, MI: American Concrete Institute; 2011.
- [13] Brenes F, Wood S, Kreger M. Anchorage requirements for grouted vertical-duct connectors in precast bent cap systems [Report no FHWA/TX-06/0-4176-1]. Austin (TX): Center for Transportation Research, University of Texas at Austin; 2006.
- [14] Mehrsoroush A, Saiidi M. Experimental and analytical seismic studies of bridge piers with innovative pipe pin column-footing connections and precast cap beams [Report no CCEER-14-07]. Reno (NV): Center for Civil Engineering Earthquake Research, Department of Civil and Environmental Engineering, University of Nevada, Reno; 2014.
- [15] Starossek U, Falah N, Lohning T. Numerical analyses of the force transfer in concrete-filled steel tube columns. *Struct Eng Mech* 2010;35(2):241–56.
- [16] Lam D, El-Lobody E. Behavior of headed stud shear connectors in composite beam. *J Struct Eng* 2005;131(1):96–107.
- [17] Hillerborg A, Modéer M, Petersson PE. Analysis of crack formation and crack growth in concrete by means of fracture mechanics and finite elements. *Cem Concr Res* 1976;6(6):773–81.
- [18] Popovics S. A numerical approach to the complete stress-strain curve of concrete. *Cem Concr Res* 1973;3(5):583–99.
- [19] Ramberg W, Osgood WR. Description of stress-strain curves by three parameters Technical note no 902 Washington, DC: National Advisory Committee for Aeronautics; 1943.
- [20] AISC. Steel construction manual. 13th ed. Chicago (IL): American Institute of Steel Construction Inc.; 2011.
- [21] Baltay P, Gjelsvik A. Coefficient of friction for steel on concrete at high normal stress. *J Mater Civ Eng* 1990;2(1):46–9.
- [22] Rabbat BG, Russell HG. Friction coefficient of steel on concrete or grout. *J Struct Eng* 1985;111(3):505–15.
- [23] Cheng ZY, Saiidi MS, Sanders D. Development of a seismic design method for reinforced concrete two-way bridge column hinges, [Report No. CCEER-06-01]2006, Center for Civil Engineering Earthquake Research, Department of Civil and Environmental Engineering, University of Nevada, Reno; Reno (NV).